Chalcogenide Letters Vol. 16, No. 10, October 2019, p. 477 - 484

STRUCTURE EFFECT ON SODIUM-ION CONDUCTION PROPERTISE OF $GeSe_2$-Ga_2Se_3-Sb_2Se_3-NaI CHALCOGENIDE GLASSES

X. Y. LIU[a,b], C. M. CHENG[a,b], C. G. LIN[a,b,*]
[a]*Laboratory of Infrared Materials and Devices, The Research Institute of Advanced Technologies, Ningbo University, Ningbo 315211, P. R. China*
[b]*Key Laboratory of Photoelectric Detection Materials and Devices of Zhejiang Province, Ningbo 315211, P. R. China*

All-solid-state rechargeable sodium ion batteries are critical for future energy storage applications, and thus new solid electrolytes with superior performance are being continuously explored. In this work, chalcogenide glassy and glass-ceramic samples with compositions of $40GeSe_2$-$(30-x)Ga_2Se_3$-xSb_2Se_3-30NaI (x=0, 2.5, 5, 7.5, and 10) were prepared and characterized through various techniques. The maximum room-temperature sodium-ion conductivity is obtained to be 1.27×10^{-6} S/cm for $40GeSe_2$-$30Ga_2Se_3$-30NaI sample. The compositional dependence of structural evolution is studied by Raman spectra. The correlation between sodium-ion conduction property and structure is discussed, which would provide further understanding for the structural effect on sodium-ion conduction properties of chalcogenide glasses.

(Received June 23, 2019; Accepted October 11, 2019)

Keywords: Chalcogenide glasses, Solid electrolytes, Ionic conductivity, Sodium-ion conduction

1. Introduction

In recent years, the development of new solid-state rechargeable battery materials has caused a wide range of research booms. Solid electrolytes with high ionic conductivity and wide electrochemical windows are one of the key materials for all-solid-state rechargeable batteries [1, 2]. Chalcogenide solid electrolytes have received particular attention due to their excellent thermal/chemical stability and fast ionic conduction properties [3, 4]. Sodium and lithium belong to the same group of elements, and there are many similarities in their chemical properties. The accumulated experience of Li^+ ion related materials has a good guiding significance for the exploration of Na^+ ones. The study of sodium ionic solid electrolytes has gradually increased and good progress has been made [5]. In 2012, A. Hayashi et al. demonstrated the observation of a conductivity of up to 2×10^{-4} S/cm in a chalcogenide glass-ceramic containing Na_3PS_4 crystal phase [6]. When the sample was re-prepared with higher purity raw materials in 2014, its conductivity increased to 4.6×10^{-4} S/cm [7]. This value is the best sodium ionic conductivity in chalcogenide glass solid electrolyte reported so far. However, the conductivity is still several orders of magnitude lower than that of oxide solid electrolytes such as β-alumina (Al) and NASICON-type

*Corresponding author: linchanggui@nbu.edu.cn

$Na_3Zr_2Si_2PO_{12}$ [8]. Therefore, it is of great significance to unravel the structural effect on ionic conduction properties of chalcogenide glasses and to search a Na^+ ion chalcogenide solid electrolyte with high conductivity.

Based on previous systematic studies on the Na^+ ion conduction behavior of glass and glass-ceramics in the $GeSe_2$-Ga_2Se_3-NaI system, it was found that the halide NaI was acted as network modification, and its content had a direct influence on the conductivity [9, 10]. When NaI content is small, the electrical conductivity of the glass material rises with the increase of the Na^+ ion concentration. In this situation, the mobile ions fill in the gaps among the structural units of network structure, and only increase with the increasing Na^+ ion concentration. After NaI content reaches to a certain value, the conductivity increases exponentially with further addition of Na^+ ion content. With the continuously increasing amount of NaI, the iodine would destroy [Ge(Ga)Se_4] and [Se_3Ge(Ga)-Ge(Ga)Se_3] group, break the giant molecular chain that formed network structure, and make the glass network structure "loose". This effect creates channels that are more conducive for ion migration, thus reduces the activation energy of ionic conduction and contributes to the exponential increase of the conductivity [11, 12].

This work is to provide further understanding for the structural effect on sodium-ion conduction property of chalcogenide glasses [13, 14]. Based on 40$GeSe_2$-30Ga_2Se_3-30NaI chalcogenide glass, Sb_2Se_3 is selected to substitute the network intermediate Ga_2Se_3. In the 40$GeSe_2$-(30-*x*)Ga_2Se_3-*x*Sb_2Se_3-30NaI system, with increasing Sb_2Se_3, the glass structure is possible to be loose and the possible formation of ionic transportation channels that are more conducive to ion migration is a worthwhile research direction [15, 16]. Together with the thermal and mechanical properties characterized by differential scanning calorimetry (DSC) and Vickers indentation, sodium-ion conduction properties of these samples are discussed with the compositional evolution of structure.

2. Experimental

Bulk samples with the compositions of 40$GeSe_2$-(30-*x*)Ga_2Se_3-*x*Sb_2Se_3-30NaI (*x*=0, 2.5, 5, 7.5, and 10) were elaborated *via* a traditional melt-quenching method. GGSN*x* is delegated for the samples with different Sb_2Se_3 content in the following context. Raw materials of high purity Ge (5N), Ga (5N), Sb (5N), Se (5N), and NaI (3N) were weighted and placed in silica ampoules, which were subsequently sealed under a vacuum of ~10^{-3} Pa. The ampoules of 9 mm inner diameter were shifted into rocking furnace, and then heated slowly to 950 °C and maintained for 12h. The melts were quenched in cold water and annealed for 4h to minimize inner constraints. Rod samples were obtained and finally cut into discs followed by double-sided polishing with a thickness of 1.5 mm.

Glass density was calculated based on Archimedes principle by comparing the difference of sample weights in air and in distilled water with an accuracy ±0.001 g/cm^3. Thermal analysis was carried out through a DSC (TA Q2000, USA) with a heating rate 10 °C/min. Based on the heat flow curves, glass transition temperature (T_g), onset temperature (T_x) and peak temperature (T_p) of crystallization peak were determined with an accuracy of ±1 °C. The near-IR photos of glasses were obtained by infrared microscope featuring 940 nm infrared LED lighting (AM413FI2TA, AnMo Electronics Corporation). Microhardness hardness (H_v) was measured by using a Vickers

microindenter (Hengyi MH-3, Shanghai, China) with a charge of 100 g for 5 s. The experimental error on H_v was about ±0.02 GPa..

The amorphous nature of samples and the precipitated crystalline phases were confirmed by X-ray diffraction (XRD, D2 Phaser, Bruker, Germany) using CuKa radiation with a step width of 0.02 °. The diffraction patterns were taken in the 2θ range of 10-70 ° under Bragg conditions. Raman spectra of bulk samples were collected in 100-400 cm^{-1} range by using a Raman spectroscopy (Renishaw InVia, England) equipped with a LD laser operating at 785 nm. The spectral resolution was ~1 cm^{-1}. The conductivity of the material was tested by AC impedance method using an electrochemical platform (Shanghai Chenhua CHI800D series). Under a dry nitrogen atmosphere, gold films were sputtered on both sides of the samples as electrodes for impedance measurements. The impedance measurements were taken from room temperature to 200 °C.

3. Results and discussion

The physical properties of $GeSe_2$-Ga_2Se_3-NaI system has been well investigated in our previous work [13]. Herein the composition of 40$GeSe_2$-30Ga_2Se_3-30NaI is specially selected as base sample, because it has been learned to possess superior sodium-ion conduction property. Sb_2Se_3 was added to substitute the Ga_2Se_3 component, in order to study the compositional dependence structural evolution and sodium-ion conduction properties.

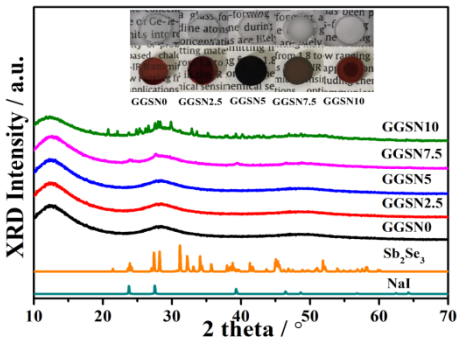

Fig. 1 XRD patterns of samples in 40$GeSe_2$-(30-x)Ga_2Se_3-xSb_2Se_3-30NaI (GGSNx) system, x =0, 2.5, 5, 7.5 and 10, respectively. The standard JCPDS cards of NaI and Sb_2Se_3 are also included.

Fig. 1 displays XRD patterns of 40$GeSe_2$-(30-x)Ga_2Se_3-$x$$Sb_2Se_3$-30NaI ($x$=0, 2.5, 5, 7.5, and 10) samples. For the samples containing low Sb_2S_3 content (x<7.5), broad diffraction peaks are observed, indicating their amorphous nature. With the further substitution of Ga_2Se_3 by Sb_2Se_3, diffraction peaks belonging to crystallites grow from the diffuse X-ray peaks. NaI crystallites are precipitated initially (x=7.5), and then Sb_2Se_3 crystal phase is also separated for x=10. This agrees with the observation of near-IR images as displayed in the inset of Fig. 1. Three glassy samples are homogenous and IR transparent, whereas the samples of x≥7.5 are devitrified.

Fig. 2 shows the DSC curves of $40GeSe_2$-$(30-x)Ga_2Se_3$-xSb_2Se_3-30NaI glassy and partially-crystallized samples. The temperatures T_g, T_x, and the common stability criterion of $\Delta T=T_x-T_g$ are given in Table 1. It is obvious that T_g decreases with the increasing Sb_2Se_3 content, indicating the loosing connectivity of glassy network caused by the substitution of Ga_2S_3 by Sb_2S_3. And the decreasing ΔT also suggests the declining thermal stability of the samples, which is in accordance with the observation of crystallization in GGSN7.5 and GGSN10 samples (Fig. 1).

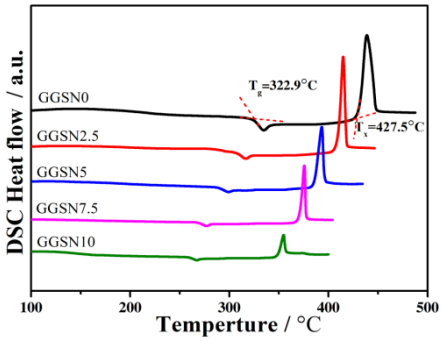

Fig. 2 DSC curve of $40GeSe_2$-$(30-x)Ga_2Se_3$-xSb_2Se_3-30NaI (GGSNx) samples, x=0, 2.5, 5, 7.5, and 10, respectively.

Table 1 Characteristic temperatures of T_g, T_x, and $\triangle T$, density and Vickers hardness of $40GeSe_2$-$(30-x)Ga_2Se_3$-xSb_2Se_3-30NaI (GGSNx) samples .

Samples	**Density (±0.001g·cm^{-3})**	**H_v （±0.02 GPa）**	**T_g （±1℃）**	**T_x （±1℃）**	**ΔT （℃）**
GGSN0	4.253	1.843	322.9	427.5	104.6
GGSN2.5	4.268	1.723	307.7	407.9	100.2
GGSN5	4.347	1.662	298.4	392.9	94.5
GGSN7.5	4.415	1.605	276.1	367.1	91.0
GGSN10	4.496	1.103	264.7	351.4	86.7

The values of density and Vickers (H_v) hardness are also collected in Table 1, and plotted as a function of Sb_2Se_3 concentration, as shown in Fig. 3. The density of samples increases with the increasing x, while the Vickers hardness decreases. The increasing density is due to the fact that the mass of antimony atoms is greater than that of gallium. The decreasing hardness is possibly originated from the variation of glassy network structure. Similarly, the addition of Sb_2Se_3 leads to the formation of three-coordinated [$SbSe_3$] pyramids, which replace for the [Se_3Ga-$GaSe_3$] structural units [17]. It would lead to the loosing of structural network. The structural evolution will be discussed below by the analysis of Raman spectra.

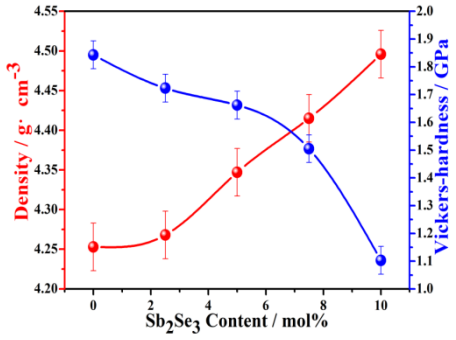

Fig. 3 Variation of the density and Vickers hardness of 40GeSe$_2$-(30-x)Ga$_2$Se$_3$ -xSb$_2$Se$_3$-30NaI (GGSNx) samples, x =0, 2.5, 5, 7.5, and 10, respectively.

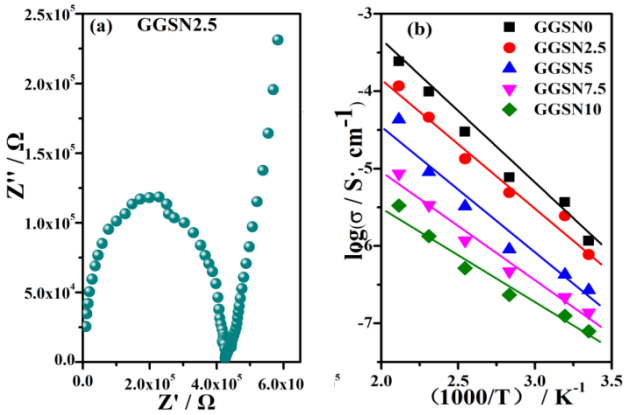

Fig. 4. (a) Nyquist plot at room temperature (25 °C) of the sample 40GeSe$_2$-27.5Ga$_2$Se$_3$-2.5Sb$_2$Se$_3$-30NaI. (b) Arrhenius plots of the ionic conductivities of glass samples.

Fig. 4 (a) gives the Nyquist impedance spectrum of the sample 40GeSe$_2$-27.5Ga$_2$Se$_3$-2.5Sb$_2$Se$_3$-30NaI at room temperature (25 °C). The first semicircle is attributed to the bulk resistance, R [18]. The intersection point with the real axis is considered to be the specific value of the bulk resistance; the subsequent slashes are called the Warburg effect. Ionic conductivity can be calculated by $\sigma=l/(R\times S)$, where l is the thickness of the sample and S is the effective area of the electrode (Au film). Figure 4(b) plots the calculated σ_{ac} as a function of temperature. It is clear that all the sodium ionic conductivities (σ_{ac}) of the studied samples follows the Arrhenius equation, $\sigma_{ac}(T)=\sigma_0\exp(-E_\alpha/RT)$, within the measured temperature ranges.

Fig. 5 shows the compositional dependence of ionic conductivity for the 40GeSe$_2$-(30-x)Ga$_2$Se$_3$-xSb$_2$Se$_3$-30NaI glasses. With the increasing Sb$_2$Se$_3$ amount from 0 mol% to 5 mol%, the sodium ionic conductivities (σ_{ac}) of the studied samples decreases rapidly, while decreases slowly for the samples with the Sb$_2$S$_3$ contents of 7.5 and 10 mol%. The variation of activation energies of conduction, E_α, which were obtained from the slope of the Arrhenius plots (Fig. 4(b)), as a function of Sb$_2$S$_3$ content. Contrary to the variation of σ_{ac}, E_α remains almost unchanged for the samples with the Sb$_2$Se$_3$ amount lower than 7.5 mol%, whereas it decreases with the further increasing Sb$_2$Se$_3$.

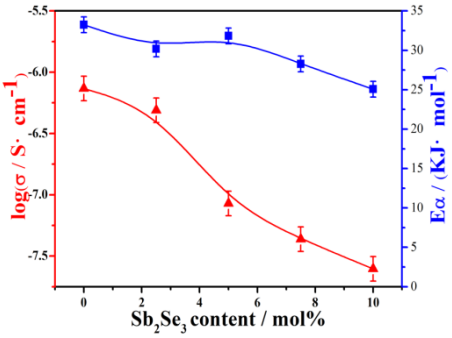

Fig. 5. Ionic conductivity (25°C) and activation energy of ionic conduction, E_α, of $40GeSe_2$-(30-x)Ga_2Se_3-xSb_2Se_3-30NaI (GGSNx) samples as a function of Sb_2Se_3 content.

To explain the structural evolution, Raman spectra were recorded as presented in Fig. 6. Based on the previous investigations of Raman spectra in $GeSe_2$–Ga_2Se_3–NaI glasses, the most intense band located at 200 cm^{-1} is assigned to the overlap of $\nu_1(A_1)$ symmetric stretching modes of corner-sharing [Ge(Ga)$Se_{4-\beta}I_\beta$] tetrahedral [12, 13]. The shoulder at 215 cm^{-1} is attributed to vibration $\nu^c_1(A^c_1)$ of edge-sharing [Ge(Ga) $Se_{4-\beta}I_\beta$] tetrahedra. The small band at 243 cm^{-1} might be associated with the presence of homopolar Se–Se bonds that is formed to compensate the slight local shortage of Sn. The band near 310 cm^{-1} is due to $\nu_3(F_2)$ asymmetric vibration modes of [$GeSe_{4-\beta}I_\beta$] [17, 19]. Through a perusal of Fig. 6, the decreasing Raman band at 168 cm^{-1} was observed with the substitution of Ga_2Se_3 by Sb_2Se_3. As we know, the existence of iodine partially replaces Se, resulting in the formation of the mixed-anion units of [$I_\beta Se_{3-\beta}$Ge(Ga)-(Ga)$GeSe_{3-\beta}I_\beta$] (β=1~3) that located around 168 cm^{-1}. The decreasing band at 168 cm^{-1} suggests that the amount of [$I_\beta Se_{3-\beta}$Ge(Ga)-(Ga)$GeSe_{3-\beta}I_\beta$] (β=1~3) structural units decreases. It is due to that, with the substitution of Ga_2Se_3 by Sb_2Se_3, new [$SbSe_{3-\beta}I_\beta$] units are formed at the dissipation of [$I_\beta Se_{3-\beta}$Ge-$GeSe_{3-\beta}I_\beta$] (x=1~3) [9].

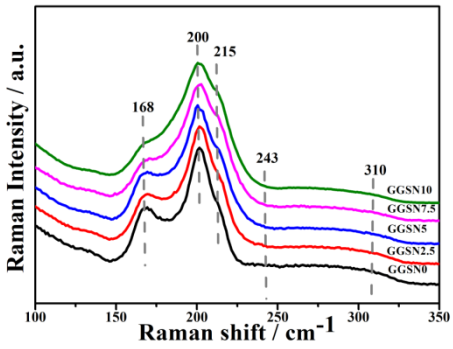

Fig. 6. Raman spectra of the glassy matrices of$40GeSe_2$-(30-x)Ga_2Se_3-xSb_2Se_3-30NaI (GGSNx), x =0, 2.5, 5,7.5, and10, respectively.

With the constant NaI content of 30 mol%, the substitution of Ga_2Se_3 by Sb_2Se_3 leads to the precipitation of NaI and Sb_2Se_3 (Fig. 1). It indicates that the [$I_\beta Se_{3-\beta}$Ge(Ga)-(Ga)$GeSe_{3-\beta}I_\beta$] (β=1~3) structural unit has much larger solubility of alkali halide that the [$SbSe_{3-\beta}I_\beta$]. And the

formation of three-coordination [$SbSe_{3-\beta}I_\beta$] leads to the loosing connectivity of structural network of glassy matrices. This structural variation contributes to the decreasing T_g and H_v as show in Figs. 2 and 3.

The variation of sodium-ion conduction properties, as shown in Fig. 5, is originated from not only the compositional changing but also the precipitation of crystallites. Firstly, with the increasing Sb_2Se_3, the solubility of NaI is lowered, which leads to the precipitation of NaI crystals. The precipitated NaI crystal not only blocks the ion transport channel, but also fixes the mobile Na^+ ions in the crystal. This is responsible for the nonlinear variation of sodium ionic conductivities as shown in Fig. 5. For the glassy samples ($x \leqslant 5$), the three-coordinated units of [$SbSe_{3-\beta}I_\beta$] with a smaller volume were replaced by the formation of [$I_\beta Se_{3-\beta}Ge(Ga)$-$(Ga)GeSe_{3-\beta}I_\beta$] in the network structure. The free volume of network structure of

$40GeSe_2$-$(30-x)Ga_2Se_3$-xSb_2Se_3-30NaI (x=0, 2.5, 5) shrinks with the increasing [$SbSe_{3-\beta}I_\beta$], leading to the narrowing of the transportation channel for mobile sodium ions [20, 21]. Therefore, it results in the decreased ionic conductivities, but their activation energy of ionic conduction (E_α) remains steadily.

4. Conclusions

$40GeSe_2$-$(30-x)Ga_2Se_3$-xSb_2Se_3-30NaI (x=0, 2.5, 5, 7.5, and 10) samples were prepared *via* a melt-quenching method. Glassy samples can be obtained when Sb_2Se_3 content is lower than 5 mol%, whereas NaI and Sb_2Se_3 crystallites would be precipitated in the samples of 7.5 and 10 mol% Sb_2Se_3. The ion conduction behavior was systematically studied by impedance measurement. The results of Raman spectra suggest that with the substitution of Ga_2Se_3 by Sb_2Se_3, new [$SbSe_{3-\beta}I_\beta$] units are formed at the dissipation of [$I_\beta Se_{3-\beta}Ge$-$GeSe_{3-\beta}I_\beta$] (β=1~3). The three-coordinated units of [$SbSe_{3-\beta}I_\beta$] have a smaller volume than that of [$I_\beta Se_{3-\beta}Ge(Ga)$-$(Ga)GeSe_{3-\beta}I_\beta$], leading to the narrowing of the transportation channel for mobile sodium ions. In addition, the presence of NaI and Sb_2Se_3 crystallites not only leads to the decreasing of ionic conductivity, but also the activation energy of ionic conduction.

Acknowledgements

This work is financially supported by the National Natural Science Foundation of China (Grant Nos. 51702172 and 61605093), Open Fund of the State Key Laboratory of Luminescent Materials and Devices (South China University of Technology, Grant Nos. 2018-skllmd-11), Natural Science Foundation of Ningbo (Grant Nos. 2018A610042), Science Research Fund Project of Ningbo University (Grant Nos. XYL18015), and is sponsored by the K. C. Wong Magna Fund in Ningbo University.

References

[1] K. Yang, Z. Liao, Z. Zhang, L. Yang, S. I. Hirano, Material Letters **236**, 554 (2019).
[2] C. Yu, J. Hageman, S. Ganapathy, L. van Eijck, L. Zhang, K. R. Adair, X. Sun,

M. Wagemaker, Journal of Material Chemistry A **7**, 10412 (2019).
[3] J. E. Shelby, Introduction to Glass Science and Technology, Royal Society of Chemistry, 2005.
[4] W. M. Haynes, CRC handbook of chemistry and physics, CRC press, 2014.
[5] A. Hayashi, K. Noi, A. Sakuda, M. Tatsumisago, Nature Communication **3**, 856 (2012).
[6] A. Hayashi, K. Noi, N. Tanibata, M. Nagao, M. Tatsumisago, Journal of Power Sources **258**, 420 (2014).
[7] A. Hooper, Journal of Physics D-Applied Physics **10**, 1487 (1977).
[8] H. Khireddine, P. Fabry, A. Caneiro, B. Bochu, Sensors and Actuators B-Chemical **40**, 223 (1997).
[9] G. Tang, C. Liu, Z. Yang, L. Luo, W. Chen, Journal of Non-Crystalline Solids **355**, 1585 (2009).
[10] B. T. Ahn, R. A. Huggins, Materials Research Bulletin **24**, 889 (1989).
[11] R. Haisty, H. Krebs, Journal of Non-Crystalline Solids **1**, 399 (1969).
[12] L. Calvez, P. Lucas, M. Rozé, H. Ma, J. Lucas, X. Zhang, Applied Physics A-Materials Science & Processing **89**, 183 (2007).
[13] S. Zhai, L. Li, F. Chen, Q. Jiao, C. Rüssel, C. Lin, Journal of the American Ceramic Society **98**, 3770 (2015).
[14] X. Huang, Q. Jiao, C. Lin, H. Ma, X. Zhang, E. Zhu, X. Liu, S. Dai, T. Xu, Scientific Reports **8**, 1699 (2018).
[15] M. Zhang, A. Yang, Y. Peng, B. Zhang, H. Ren, W. Guo, Y. Yang, C. Zhai, Y. Wang, Z. Yang, Materials Research Bulletin **70**, 55 (2015).
[16] G. Tang, Z. Yang, L. Luo, W. Chen, Journal of the American Ceramic Society **91**, 1686 (2008).
[17] K. Maeda, T. Sakai, K. Sakai, T. Ikari, M. Munzar, D. Tonchev, S. Kasap, G. Lucovsky, Journal of Materials Science-Materials Electronics **18**, 367 (2007).
[18] E. Kelder, M. Jak, F. De Lange, J. Schoonman, Solid State Ionics **85**, 285 (1996).
[19] A. Mao, B. Aitken, R. Youngman, D. Kaseman, S. Sen, The Journal of Physical Chemistry B, **117**, 16594 (2013).
[20] J. H. Lee, W. H. Lee, J. K. Park, J. H. Yi, S. Y. Shin, B. J. Park, B. So, J. Heo, J. H. Choi, H. J. Kim, Y. G. Choi, Journal of Non-Crystalline Solids **431**, 41 (2016).
[21] Y. S. Tveryanovich, A. V. Bandura, S. V. Fokina, E. N. Borisov, R. A. Evarestov, Solid State Ionics **294**, 82 (2016).